

REPORT DOCUMENTATION PAGE

Form Approved
OMB No. 0704-0188

Public reporting burden for this collection of information is estimated to average 1 hour per response, including the time for reviewing instructions, searching existing data sources, gathering and maintaining the data needed, and completing and reviewing this collection of information. Send comments regarding this burden estimate or any other aspect of this collection of information, including suggestions for reducing this burden to Department of Defense, Washington Headquarters Services, Directorate for Information Operations and Reports (0704-0188), 1215 Jefferson Davis Highway, Suite 1204, Arlington, VA 22202-4302. Respondents should be aware that notwithstanding any other provision of law, no person shall be subject to any penalty for failing to comply with a collection of information if it does not display a currently valid OMB control number. **PLEASE DO NOT RETURN YOUR FORM TO THE ABOVE ADDRESS.**

1. REPORT DATE (DD-MM-YYYY) 27 July 2016		2. REPORT TYPE Conference Paper		3. DATES COVERED (From - To) 30 June 2016 - 27 July 2016	
4. TITLE AND SUBTITLE Multi-Fidelity Framework for Modeling Combustion Instability				5a. CONTRACT NUMBER	
				5b. GRANT NUMBER	
				5c. PROGRAM ELEMENT NUMBER	
6. AUTHOR(S) Huang, C., Anderson, W., Merkle, C. and Sankaran, V.				5d. PROJECT NUMBER	
				5e. TASK NUMBER	
				5f. WORK UNIT NUMBER Q12J	
7. PERFORMING ORGANIZATION NAME(S) AND ADDRESS(ES) AND ADDRESS(ES) Air Force Research Laboratory (AFMC) AFRL/RQR 5 Pollux Drive Edwards AFB, CA 93524-7048				8. PERFORMING ORGANIZATION REPORT NO.	
9. SPONSORING / MONITORING AGENCY NAME(S) AND ADDRESS(ES) Air Force Research Laboratory (AFMC) AFRL/RQR 5 Pollux Drive Edwards AFB, CA 93524-7048				10. SPONSOR/MONITOR'S ACRONYM(S)	
				11. SPONSOR/MONITOR'S REPORT NUMBER(S) AFRL-RQ-ED-AB-2016-198	
12. DISTRIBUTION / AVAILABILITY STATEMENT Approved for Public Release; Distribution Unlimited. PA Clearance Number: 16327 Clearance Date: 7/12/2016					
13. SUPPLEMENTARY NOTES For presentation at AIAA Propulsion and Energy Conference 2016; Salt Lake City, UT July 25-27, 2016					
14. ABSTRACT A multi-fidelity framework for combustion instability modeling is established by integrating a reduced-order model (ROM) for combustion response into the linearized Euler equations. The ROM is developed from CFD simulations of periodic forcing on a reduced domain using Galerkin's method to reduce the high-order PDEs to a lower-order ODE system via POD eigen-bases generated from the reduced-domain dataset. Evaluations of the framework are performed based on simplified test problems for a model rocket combustor showing distinguishable instability behaviors. The coupling between the ROM and the Euler equations requires two-way information transfer between the two systems. Results show that the fraction of the complete domain represented by the ROM can be chosen to simplify the interaction between the two levels of solution. The multi-fidelity model is capable of capturing the overall instability trends although some discrepancies due to unstable generic responses arising from the reduced-domain simulations.					
15. SUBJECT TERMS N/A					
16. SECURITY CLASSIFICATION OF:			17. LIMITATION OF ABSTRACT	18. NUMBER OF PAGES	19a. NAME OF RESPONSIBLE PERSON
a. REPORT	b. ABSTRACT	c. THIS PAGE			V. Sankaran
Unclassified	Unclassified	Unclassified	SAR	21	19b. TELEPHONE NO (include area code) N/A

Standard Form
298 (Rev. 8-98)
Prescribed by ANSI
Std. Z39.18

Multi-Fidelity Framework for Modeling Combustion Instability

Cheng Huang^{*}, William E. Anderson[†], Charles L. Merkle[‡]

Purdue University, West Lafayette, IN, 47907

and

Venkateswaran Sankaran[§]

Air Force Research Laboratory (AFRL), Edwards AFB, CA, 93524

A multi-fidelity framework for combustion instability modeling is established by integrating a reduced-order model (ROM) for combustion response into the linearized Euler equations. The ROM is developed from CFD simulations of periodic forcing on a reduced domain using Galerkin’s method to reduce the high-order PDEs to a lower-order ODE system *via* POD eigen-bases generated from the reduced-domain dataset. Evaluations of the framework are performed based on simplified test problems for a model rocket combustor showing distinguishable instability behaviors. The coupling between the ROM and the Euler equations requires two-way information transfer between the two systems. Results show that the fraction of the complete domain represented by the ROM can be chosen to simplify the interaction between the two levels of solution. The multi-fidelity model is capable of capturing the overall instability trends although some discrepancies due to unstable generic responses arising from the reduced-domain simulations.

I. Introduction

Combustion instabilities arising from organized pressure oscillations driven by hydrodynamic coupling to the heat release often occur in practical combustors. Problem complexity is enhanced by the intense, but distributed, nature of the heat release, the complex chemical reactions and companion large numbers of molecular species produced by combustion of realistic propellants, highly complicated geometries and multiple inlet ports. Though modern computational capability offers the potential for moving beyond the empirically-based design analyses of

^{*} Postdoctoral Research Assistant, School of Aeronautics and Astronautics and Member AIAA.

[†] Professor, School of Aeronautics and Astronautics and Associate Fellow AIAA.

[‡] Professor Emeritus.

[§] Senior Scientist, Rocket Propulsion Division and Senior Member AIAA.

the past, simulations of full-scale geometries for engineering analysis are still far out of reach. High fidelity simulations of smaller domains can, however, be potentially used to derive reduced order models of the unsteady combustion response that can in turn provide generic descriptions of the complex couplings and thereby predict the combustion stability of full-scale configurations.

Research efforts in combustion response function development can be categorized into physics-based and mathematics-based efforts. Physics-based approaches generally adopt a reduced fidelity model such as a wave equation in combination with combustion response functions that are derived through physical intuition. Usually this means that the unsteady heat release is expressed in terms of the fluctuations of the local pressure and velocity field. Such approaches include the Flame Transfer Function (FTF) and the Flame Describing Function (FDF) methods [1], widely used in premixed combustion for gas turbine engine application [2-5]. You et al. [6] developed an analytical model based on a level-set flamelet model to obtain the combustion response of turbulent premixed flames to acoustic oscillations. However, the generality of such approaches are not well established especially in the context of the large amplitude oscillations that are characteristic rocket combustors. More recently, Popov and Sirignano [7] successfully demonstrated the modeling of transverse combustion instability in a rectangular rocket combustor [8] using a reduced-fidelity simulation approach. However, there are several ad-hoc simplifications in the model and their general applicability to other rocket configurations is not established.

In this paper, we focus on the mathematics-based approach based on formal model reduction techniques [10-12] that couple model decomposition (e.g. Proper Orthogonal Decomposition) and projection (e.g. Galerkin) methods. Such model reduction techniques have been proven to be efficient for reducing the higher-order partial differential equations (PDE) to ordinary differential equations (ODE) and the resulting reduced order models (ROM) have been applied to non-reacting flow problems including flow control [13-15] and unsteady aeroelasticity [16, 17]. Recent studies have extended ROMs to combustion problems [18, 19]. Preliminary explorations of the POD/Galerkin technique have been carried out by the present authors for both a model scalar equation [20], and the Euler system of equations [21, 22]]. These studies have established a basic approach for ROM construction and its characteristics for frequency-dependent problems. The present work seeks to extend the ROM approach to a multi-fidelity framework for the solution of representative combustion stability problems.

The main objective of the current paper is to demonstrate a multi-fidelity framework for modeling combustion instability problems. The underlying idea of our approach involves two distinct stages: the first stage is to construct the ROM through suitable training for a representative class of *reduced-domain* problems, and the second stage is to embed the ROM within a linearized Euler equation solution in order to predict combustion instability occurrence for the real *full-domain* configuration. In the latter stage, the ROM provides the combustion response source terms in the Euler equations and, in that sense, it resembles the FTF/FDF approaches discussed earlier. However, the difference lies in the use of the ROM to define the combustion response terms.

A related secondary objective of this study is to examine the accuracy of using different reduced problems in the ROM construction phase. Specifically, we use a representative longitudinal mode experimental combustor [9] that demonstrates both stable and unstable operation depending upon the length of the injector post. In the ROM

construction stage, we employ different reduced-domains involving just the injector section in order to train the ROM. We examine the effects of introducing different boundary condition perturbations in order to represent the response of the injector to self-excited oscillations in the full combustor. In each case, the resulting ROM is subsequently embedded within the full-domain injector-combustor configuration and the accuracy of the predictions is evaluated.

The computational savings of this multi-fidelity approach comes from the fact that the expensive simulations are restricted to the reduced domain problem during the ROM training process (i.e., the first stage). In contrast, the full-domain problem is solved very efficiently (in the second stage) using the previously constructed ROM. In general, the first stage would involve high-fidelity simulations such as large eddy simulation (LES) or detached eddy simulations (DES), while the second stage utilizes the ROM embedded within a reduced fidelity solution such as the Euler equations. We note that, for the purposes of this initial demonstration, we utilize one-dimensional Euler solutions in both stages. This not only allows for more efficient calculations of the first stage, but it also has the further advantage of providing benchmark-quality solutions that facilitate detailed accuracy assessments of the proposed procedure.

The remainder of the paper is organized as follows. In Section II, we present the governing Euler equations with a modeled combustion source term and the forcing function and boundary conditions used. In addition, we also present the Galerkin formulation and the POD techniques for deriving the ROM for the linearized version of the Euler equations. In Section III, we describe the multi-fidelity framework approach including a definition of the test problem, the training processes of the POD-based ROM and the overall method for inserting the constructed ROM into the linearized-Euler framework. In Section IV, we present the computational results of our studies. We explore the effects of using different reduced-domain geometries for training the ROMs and, in particular, deduce the number of ROM solutions required to fully capture the acoustic wave response of the injector. We also consider the case where the reduced-domain includes the full injector post and contrast those results with the previous reduced-domain studies. In each case, we compare the predictions of the proposed multi-fidelity framework with those obtained from the baseline governing equations to establish the ROM performance. In the final section, we provide concluding remarks and suggest directions for continued research.

II. Formulation

A. Governing equations

The governing equations are the quasi-one-dimensional unsteady Euler equations with a single-step chemical reaction and a specified reaction distribution,

$$\frac{\partial \mathbf{Q}}{\partial t} + \frac{\partial \mathbf{E}}{\partial x} = \mathbf{H} + \mathbf{H}_f + \mathbf{H}_q \quad (1)$$

where,

$$\mathbf{Q} = \begin{pmatrix} \rho A \\ \rho u A \\ e A \\ \rho Y_{ox} A \end{pmatrix}, \mathbf{E} = \begin{pmatrix} \rho u A \\ (\rho u^2 + p) A \\ (e + p) A \\ \rho u Y_{ox} A \end{pmatrix}, \mathbf{H} = \begin{pmatrix} 0 \\ p \frac{dA}{dx} \\ 0 \\ 0 \end{pmatrix}, \mathbf{H}_f = \begin{pmatrix} \dot{\omega}_f \\ \dot{\omega}_f \bar{u} \\ \dot{\omega}_f \left(\bar{h}_0 - \frac{\bar{p}}{\bar{\rho}} \right) \\ -\dot{\omega}_{ox} \end{pmatrix}, \mathbf{H}_q = \begin{pmatrix} 0 \\ 0 \\ \dot{q}''' \\ 0 \end{pmatrix}.$$

Here x and t are the space and time variables, ρ is the density, u is the velocity, e is the total energy, p is the pressure, Y_{ox} is the oxidizer mass fraction and $A = A(x)$ is the cross-section area of the geometry. The effects of fuel addition are accounted through steady source term \mathbf{H}_f , where $\dot{\omega}_f = C_{f/O} \dot{\omega}_{ox}$ with constant $C_{f/O}$ representing fuel-to-oxidizer ratio and a sinusoidal spatial distribution is used to model the oxidizer reaction,

$$\dot{\omega}_{ox} = k_f \bar{\rho} \bar{Y}_{ox} \left(1 + \sin \left(-\frac{\pi}{2} + \frac{x - l_s}{l_f - l_s} 2\pi \right) \right), \quad (\forall l_s < x < l_f),$$

where l_s and l_f are the axial locations of the beginning and end of the combustion zone. The reaction constant k_f is selected to ensure that the oxidizer is consumed within the specified combustion zone. The unsteady combustion response is accounted in the source term, \mathbf{H}_q , using the n - τ model [23], $\dot{q}''' = n \cdot \alpha(x) \cdot p'(x, t - \tau) = n \cdot \alpha(x) \cdot (p(x, t - \tau) - \bar{p}(x))$, which relates the unsteady heat release to the pressure oscillations through an index, n and a time lag constant, τ . Here $\alpha(x)$ is a scaling function following a normal distribution, $\alpha(x) = \frac{1}{\sigma \sqrt{2\pi}} \exp \left(-\frac{(x - \mu)^2}{2\sigma^2} \right)$. This model was previously used [24] to simulate combustion instability in a longitudinal rocket combustor,

For simplicity, the linearized version of Eq. (1) is used for the studies in ROM development,

$$\bar{\Gamma}_p \frac{\partial \mathbf{Q}'_p}{\partial t} + \frac{\partial \bar{A}_p \mathbf{Q}'_p}{\partial x} = \bar{D}_p \mathbf{Q}'_p \quad (2),$$

where $\mathbf{Q}'_p = (p' \quad u' \quad T' \quad Y'_{ox})^T$, $\bar{\Gamma}_p = \left. \frac{\partial \mathbf{Q}}{\partial \mathbf{Q}_p} \right|_{\bar{\mathbf{Q}}_p}$, $\bar{A}_p = \left. \frac{\partial \mathbf{E}}{\partial \mathbf{Q}_p} \right|_{\bar{\mathbf{Q}}_p}$ and $\bar{D}_p = \left(\frac{\partial \mathbf{H}}{\partial \mathbf{Q}_p} + \frac{\partial \mathbf{H}_q}{\partial \mathbf{Q}_p} \right) \Big|_{\bar{\mathbf{Q}}_p}$.

B. Construction of POD eigen-bases for vector equations

POD eigen-bases are calculated based on the CFD solutions, $\mathbf{Q}'_p(x, t)$ obtained from Eq. (2) using the vector-valued method,

$$P(x)\mathbf{Q}'_p(x,t) \approx \sum_{n=1}^{N_p} \hat{a}_n(t) \sigma_n \Phi_n(x) = \sum_{n=1}^{N_p} \hat{a}_n(t) \sigma_n \begin{pmatrix} \phi_{p,n}(x) \\ \phi_{u,n}(x) \\ \phi_{T,n}(x) \\ \phi_{Y_{ox},n}(x) \end{pmatrix} = \sum_{n=1}^{N_p} a_n(t) \begin{pmatrix} \phi_{p,n}(x) \\ \phi_{u,n}(x) \\ \phi_{T,n}(x) \\ \phi_{Y_{ox},n}(x) \end{pmatrix} \quad (3),$$

where σ_n is the singular value of the n^{th} POD mode (scalar), $a_n(t)$ is the n^{th} POD temporal mode (scalar), and the n^{th} eigen-mode, $\Phi_n(x)$, is an orthonormal vector function,

$$\int_x \Phi_n^T(x) \Phi_n(x) dx = \begin{cases} 1, & \text{if } k = n \\ 0, & \text{otherwise} \end{cases}, \quad X = \{0 \leq x \leq L\} \quad (4).$$

It should be noted that, unlike in the scalar equation case, to obtain reasonably scaled POD eigen-bases for the vector variables, a normalization matrix $P(x)$ must be used before calculating the POD eigen-bases. Here, in this abstract, we use the maximum of the fluctuating quantities for the normalization of all four variables,

$$P(x) = \text{diag} \left(\frac{1}{p'_{\max}}, \frac{1}{u'_{\max}}, \frac{1}{T'_{\max}}, \frac{1}{Y'_{ox,\max}} \right) \quad (5),$$

where $p'_{\max} = \text{Max} \{p'(x,t)\}$, $\forall 0 \leq x \leq L$ and t so that the variations in each variable can be taken into account in relative to their maximum amplitude. To reconstruct the CFD solutions using the POD eigen-bases, the matrix $P(x)$ again needs to be included,

$$\mathbf{Q}'_p(x,t) \approx P^{-1}(x) \sum_{n=1}^{N_p} a_n(t) \begin{pmatrix} \phi_{p,n}(x) \\ \phi_{u,n}(x) \\ \phi_{T,n}(x) \\ \phi_{Y_{ox},n}(x) \end{pmatrix} \quad (6).$$

C. Model reduction of Euler equations

The application of the POD-Galerkin method to the linearized Euler equations (Eq. (2)) is briefly introduced here. Additional details can be found in Ref [20]. Upon obtaining the eigen-bases as in Eq. (3), the target governing equation is projected onto the k^{th} eigen-mode, $\Phi_k(x)$, throughout the whole computational domain. Before the projection the governing equation needs to be normalized by pre-multiplying by the matrix $P(x)$,

$$\int_x \Phi_k^T(x) P(x) \left(\frac{\partial \mathbf{Q}'_p(x,t)}{\partial t} + \bar{\Gamma}_p^{-1}(x) \frac{\partial \bar{A}_p(x) \mathbf{Q}'_p(x,t)}{\partial x} \right) dx = \int_x \Phi_k^T(x) P(x) \bar{\Gamma}_p^{-1}(x) \bar{D}_p(x) \mathbf{Q}'_p(x,t) dx \quad (7),$$

Substituting the POD expansion, Eq. (6) into Eq. (7) and using a numerical quadrature to approximate the integrals,

$$\begin{aligned}
& \sum_{n=1}^{N_p} \left\{ \sum_{i=1}^{\text{NI}} \mathbf{\Phi}_{k,i}^T P_i P_i^{-1} \mathbf{\Phi}_{n,i} \Delta x_i \right\} \dot{a}_n(t) \\
& + \sum_{n=1}^{N_p} \left\{ \sum_{i=1}^{\text{NI}} \left(\mathbf{\Phi}_{k,i}^T P_i \bar{\Gamma}_{p,i}^{-1} \left(\frac{\delta \bar{A}_p P^{-1} \mathbf{\Phi}_n}{\delta x} \right)_i - \mathbf{\Phi}_{k,i}^T P_i \bar{\Gamma}_{p,i}^{-1} \bar{D}_{p,i} P_i^{-1} \mathbf{\Phi}_{n,i} \right) \Delta x_i \right\} a_n(t) = 0
\end{aligned} \tag{8}$$

Following the model reduction procedure in Ref [20] and using a consistent discretization scheme (a 2nd-order upwind scheme is used in both CFD and ROM) to approximate the gradient term in Eq. (8), an ODE system can be obtained with the contributions from boundary conditions appearing as a source term on the right-hand-side,

$$\frac{d\mathbf{a}(t)}{dt} - L\mathbf{a}(t) = \mathbf{h}(t) \tag{9}$$

where $\mathbf{a}(t) = [a_1(t) \ \cdots \ a_k(t) \ \cdots \ a_{N_p}(t)]^T$,

$\mathbf{h}(t) = [h_1(t) \ \cdots \ h_k(t) \ \cdots \ h_{N_p}(t)]^T$ with contributions from boundary conditions, $h_m(t) = h_m\{\phi'(t)\}$,

L is the stiffness matrix which describes the dynamics of the reduced ODE system.

D. ROM stabilization through artificial dissipation

It has been shown in previous studies that a simple treatment like including additional artificial dissipation in building the ROM can be useful to eliminate the non-physical unstable modes [12]. Here the method of including the artificial dissipation is briefly introduced starting with the discretized form of the linearized model equation, Eq. (2),

$$\bar{\Gamma}_{p,i} \frac{\partial \mathbf{Q}'_{p,i}}{\partial t} \Delta x_i + (\bar{A}_p \mathbf{Q}'_p)_{i+1/2} \text{area}_{i+1/2} - (\bar{A}_p \mathbf{Q}'_p)_{i-1/2} \text{area}_{i-1/2} - \bar{D}_{p,i} \mathbf{Q}'_{p,i} \Delta x_i = 0 \tag{10}$$

where Δx_i is the size of the i^{th} cell and $\text{area}_{i+1/2}$ is the left/right faces area of the i^{th} cell. The artificial dissipation is added at the cell faces,

$$\begin{aligned}
(\bar{A}_p \mathbf{Q}'_p)_{i+1/2} &= \frac{1}{2} \left\{ (\bar{A}_p \mathbf{Q}'_p)_{i+1/2}^L + (\bar{A}_p \mathbf{Q}'_p)_{i+1/2}^R \right\} - \frac{1}{2} \beta \underbrace{|\bar{A}_p|_{i+1/2}}_{\text{Artificial Dissipations}} \left\{ (\mathbf{Q}'_p)_{i+1/2}^R - (\mathbf{Q}'_p)_{i+1/2}^L \right\} \\
(\bar{A}_p \mathbf{Q}'_p)_{i-1/2} &= \frac{1}{2} \left\{ (\bar{A}_p \mathbf{Q}'_p)_{i-1/2}^L + (\bar{A}_p \mathbf{Q}'_p)_{i-1/2}^R \right\} - \frac{1}{2} \beta \underbrace{|\bar{A}_p|_{i-1/2}}_{\text{Artificial Dissipations}} \left\{ (\mathbf{Q}'_p)_{i-1/2}^R - (\mathbf{Q}'_p)_{i-1/2}^L \right\}
\end{aligned} \tag{11}$$

It should be noted that the artificial dissipation already exists in the original CFD solutions since we are using a 2nd-order upwind discretization scheme (with $\beta = 1$), based upon which the POD eigen-basis is calculated. To increase the stabilizing influence of the ROM, different β values (>1) are used during the Galerkin projection step. By systematically varying the value of the β parameter, we can estimate how much extra artificial dissipation is needed to stabilize the ROMs.

III. Multi-Fidelity Framework

A. Overview of Test Problem

A well-documented benchmark laboratory single-element rocket combustor [9, 25, 26] is selected as the baseline test problem to assess the capability of POD/Galerkin techniques in developing a combustion response function for predictions of combustion instabilities. The combustor is designed with closed acoustic boundary conditions both upstream and downstream to generate sustainable self-excited pressure oscillations. In this paper, the computations are performed using the simplified geometry with the one-dimensional linearized Euler equation (Eq. (2)), the representative geometry setup of which is shown in Fig. 1 with three major components: oxidizer-post (variable lengths, L_{ox}), combustion chamber (variable lengths, $L_{chamber}$) and nozzle at the end. The mean flow conditions are configured the same as given in Ref [9] with chamber pressure approximately 1.47MPa. The unsteady combustion response is accounted through the n - τ model (\dot{q}''' in Eq. (1)) specified at the highlighted location in Fig. 1. For simplicity, τ value is set to zero and six different n values (0.605×10^3 , 0.805×10^3 , 1.05×10^3 , 1.205×10^3 , 1.305×10^3 and 1.405×10^3 1/s) are used to perform the computation to obtain distinguishable instability behaviors. In addition, both the lengths of oxidizer post and combustion chamber are varied for model evaluations.

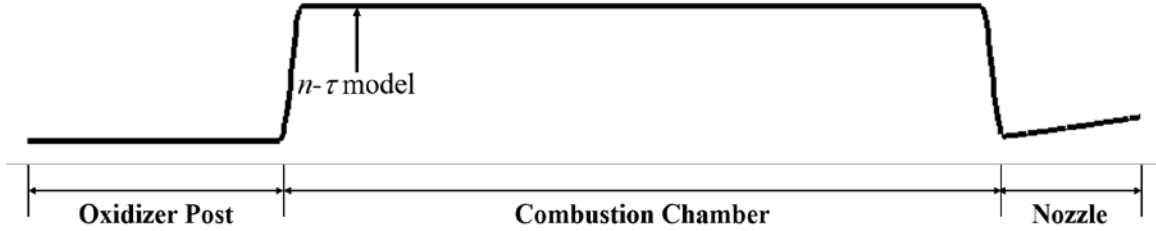


Figure 1. Overview of one-dimensional test problem using linearized Euler equations.

B. Training Process

A reduced domain is setup for the POD-based ROM development as shown in Fig. 2, containing a portion of the oxidizer post and combustion chamber in Fig. 1, covering the combustion region and expected to capture the generic combustion response. The mean flow conditions of the reduced domain are configured to be consistent with the test problem. For a typical computation, the steady state numerical solutions of Eq. (1) are computed first with a constant boundary conditions both upstream and downstream. Then the unsteady CFD solutions inside the computational domain are obtained by specifying periodic oscillations of target quantities ($\phi'(t)$), which can be inlet mass flow rate ($\dot{m}'(t)$), stagnation temperature (T^0) and back pressure (p'_{back}), about its mean value (ϕ_0),

$$\phi'(t) = \phi_0 \frac{\varepsilon}{N_f} \sum_{k=1}^{N_f} \sin(2\pi(f_0 + \Delta f)k t) \quad (12),$$

where f_0 is the initial frequency; Δf represents the fundamental frequency increment and N_f is the total number of frequencies included in the forcing function. The fundamental period T_p is determined by Δf such that $T_p = 1/\Delta f$. Note that if $\Delta f = f_0$, Eq. (12) represents a standard Fourier series although herein we generally take $\Delta f < f_0$ so that Eq. (12) differs from a Fourier series.

The solutions are tabulated and stored periodically (i.e., at several time-levels within a forcing period) thereby generating a rectangular matrix that can be used a data base for fitting eigen-bases by means of the POD procedure detailed below. The POD eigen-bases are then applied to the governing linear or non-linear PDE to derive the reduced-order ODE formulation (or ROM) following the procedure in section II.

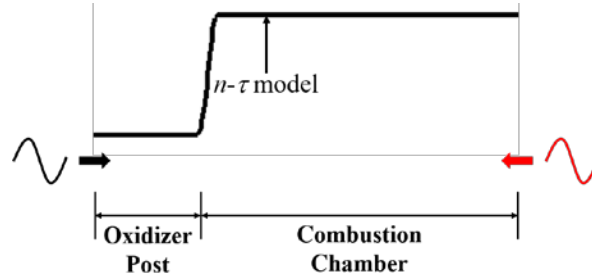


Figure 2. Training process of POD-based ROM using reduced-domain simulations.

The ROMs developed in this paper are developed by including nine frequencies ($f_0 = 500\text{Hz}$, $\Delta f = 250\text{Hz}$ and $N_f = 9$) in the boundary forcing function defined in Eq. (12). The resulting ROM characteristics is examined by the eigen-values ($\sigma + j2\pi f$) of the ODE stiffness matrix L in Eq. (9) and representative ROM spectra (trained by inlet mass flow rate perturbation with $n = 1.305 \times 10^3 \text{ 1/s}$) are shown in Fig. 3 by including different amount of artificial dissipations. It should be noted that by not including any additional dissipations ($\beta = 1$), spurious unstable eigen-mode can be observed ($\sigma > 0$) near 6500Hz and when the amount of dissipations is increased up to 1.8 times, the unstable mode is dragged back to the left-hand plane and ROM becomes numerically stable. All the ROMs used in this paper are stabilized following the same procedure.

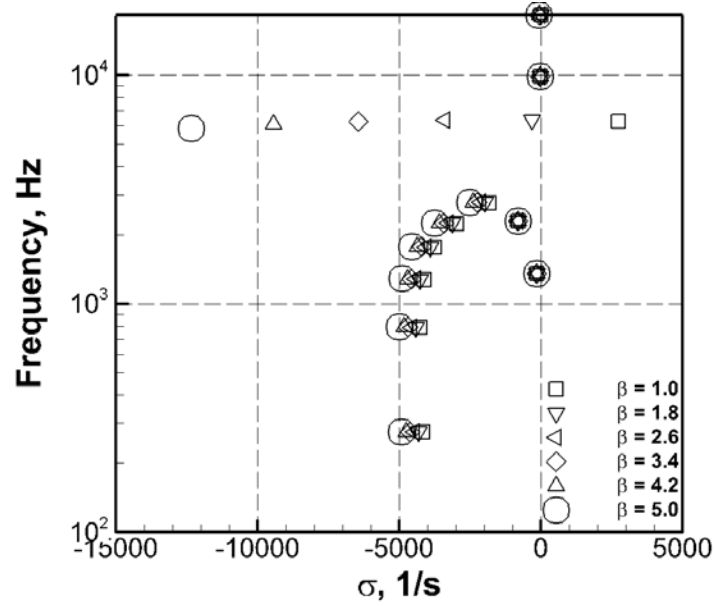


Figure 3. Eigen-value spectrum of ROM stiffness matrix by including different amounts of artificial dissipation ($n = 1.305 \times 10^3$ 1/s, ROM is trained by perturbing inlet mass flow rate).

C. Multi-fidelity Solution Methodology

The multi-fidelity framework that integrates the ROMs with the Euler solver to simulate the test problem (Fig. 1) is introduced in this section. After generating the ROMs following the training process in part B, the ROMs are then used to replace the n - τ model to describe the unsteady combustion responses within the domain bounded by the dashed line in Fig. 4.

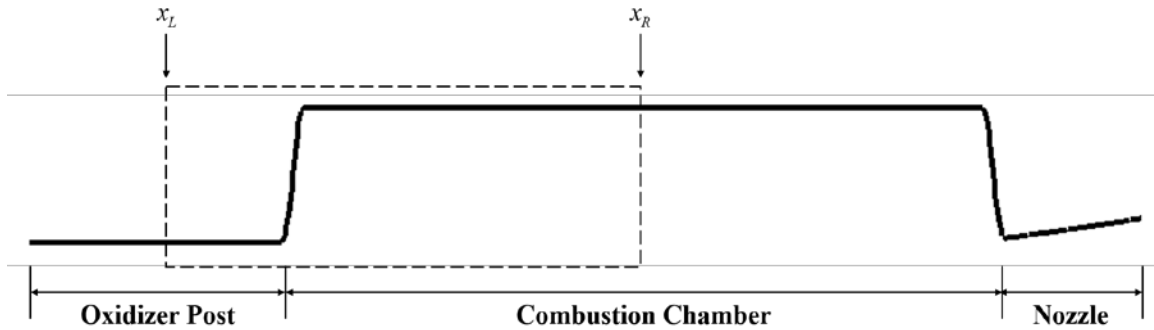


Figure 4. Overview of one-dimensional test problem using linearized Euler equations.

The overall procedures are summarized as below and it should be noted that the ROM/Euler solver integration can include multiple ROMs trained by different perturbations,

Step 1. Calculate the initial conditions, $\mathbf{a}_k(t=0)$, for the k^{th} individual ROM ODE (e.g. each ROM can trained with different perturbations) using initial CFD solutions, $\mathbf{Q}'_p(x_L \leq x \leq x_R, t=0)$ within the region covered by the reduced-domain,

$$a_{k,m}(t) = \int_{x_L}^{x_R} \Phi_{k,m}^T(x) \frac{\mathbf{Q}'_p(x, t=0)}{N_{\text{ROM}}} dx, \text{ where } \Phi_{k,m}(x) = \begin{pmatrix} \phi_{p,k,m}(x) \\ \phi_{u,k,m}(x) \\ \phi_{T,k,m}(x) \\ \phi_{Y_{ox},k,m}(x) \end{pmatrix} \text{ and } \mathbf{Q}'_p(x, t=0) = \begin{pmatrix} p'(x, t=0) \\ u'(x, t=0) \\ T'(x, t=0) \\ Y'_{ox}(x, t=0) \end{pmatrix} \quad (13),$$

where m is the mode number of POD eigen-bases, the N_{ROM} is the total number of ROMs to be integrated with the Euler solver and $\Phi_{k,m}(x)$ is the m^{th} pre-calculated POD eigen-basis for the k^{th} individual ROM using Eq. (3).

Step 2. As shown in Fig. 5, obtain the fluctuating quantities at the upstream or downstream locations in the test problem, which correspond to the boundaries of the reduced-domain (Fig. 2). The fluctuating quantities should be consistent with the ones being perturbed for ROM generation (e.g. if the ROM is trained by perturbing the downstream pressure in reduced domain, p' at location x_R needs to be extracted from the test problem as an input for the ROM ODE). Then feed the obtained fluctuating quantities, $\phi'_k(t)$, as an input to the ROM following Eq. (9).

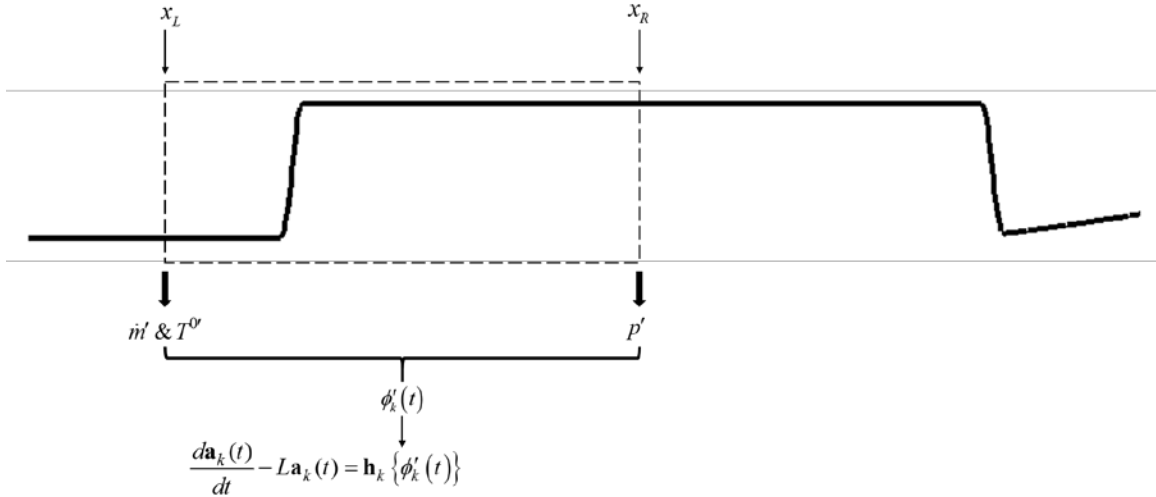


Figure 5. Schematics of integration procedure to obtain inputs for ROM ODEs.

Step 3. Solve the k^{th} ROM ODE for temporal coefficients, $\mathbf{a}_k(t)$, and obtain the corresponding solution variables,

$$\mathbf{Q}'_{p,k,\text{ROM}}(x, t), \text{ using the pre-calculated POD eigen-basis, } \Phi_{k,m}(x),$$

$$\frac{d\mathbf{a}_k(t)}{dt} - L\mathbf{a}_k(t) = \mathbf{h}_k \{\phi'_k(t)\} \Rightarrow \mathbf{a}_k(t) \Rightarrow \mathbf{Q}'_{p,k,\text{ROM}}(x,t) = \begin{pmatrix} p'_{k,\text{ROM}}(x,t) \\ u'_{k,\text{ROM}}(x,t) \\ T'_{k,\text{ROM}}(x,t) \\ Y'_{\text{ox},k,\text{ROM}}(x,t) \end{pmatrix} \approx \sum_{m=1}^{N_p} a_{k,m}(t) \Phi_{k,m}(x) \quad (14),$$

Step 4. Combine all the solution variables, $\mathbf{Q}'_{p,k,\text{ROM}}(x,t)$, from each ROM to obtain the total variable solutions,

$$\mathbf{Q}'_{p,\text{ROM}}(x,t),$$

$$\mathbf{Q}'_{p,\text{ROM}}(x,t) = \sum_{k=1}^{N_{\text{ROM}}} \mathbf{Q}'_{p,k,\text{ROM}}(x,t) \quad (15),$$

Step 5. Obtain the unsteady combustion response (input to Euler solver as the source term in energy equation)

using the \dot{q}''' expression in Eq. (1) form the total variable solutions, $\mathbf{Q}'_{p,\text{ROM}}(x,t)$,

$$\dot{q}'''_{\text{ROM}} = n \cdot \alpha(x) \cdot p'_{\text{ROM}}(x,t) \quad (16),$$

IV. Results

In this section, the multi-fidelity model framework is validated and evaluated against the baseline CFD results of the test problem (Fig. 1). Before proceeding to the detailed investigations of the reduced-order modeling approach, the key question that needs to be answered is how the ROMs should be trained and integrated with the Euler solver to get the correct instability predictions. For the initial study, a reduced-domain with $L_{\text{ox}} = 2.5''$ and $L_{\text{chamber}} = 7.5''$ is selected for the development of POD-based ROMs by applying periodic perturbations of quantities at upstream and downstream boundaries. (Note that the upstream boundary conditions are mass flow rate and stagnation temperature, while the downstream boundary condition is specified pressure.) Each boundary condition perturbation corresponds to an individual ROM and so, for the general case, there would be three ROMs for the one-dimensional test problem. It is interesting to see what the predictions would be if only one of the ROMs is used in constructing the combustion response. The geometry chosen for this study has $L_{\text{ox}} = 5.5''$ and $L_{\text{chamber}} = 15.0''$ for two different n values ($n = 1.205 \times 10^3$ and 1.305×10^3 1/s). As shown in Fig. 6, amplitude decay (stable) and growth (unstable) can be seen in the predicted pressure fluctuations from baseline CFD solutions for the lower and higher n values respectively.

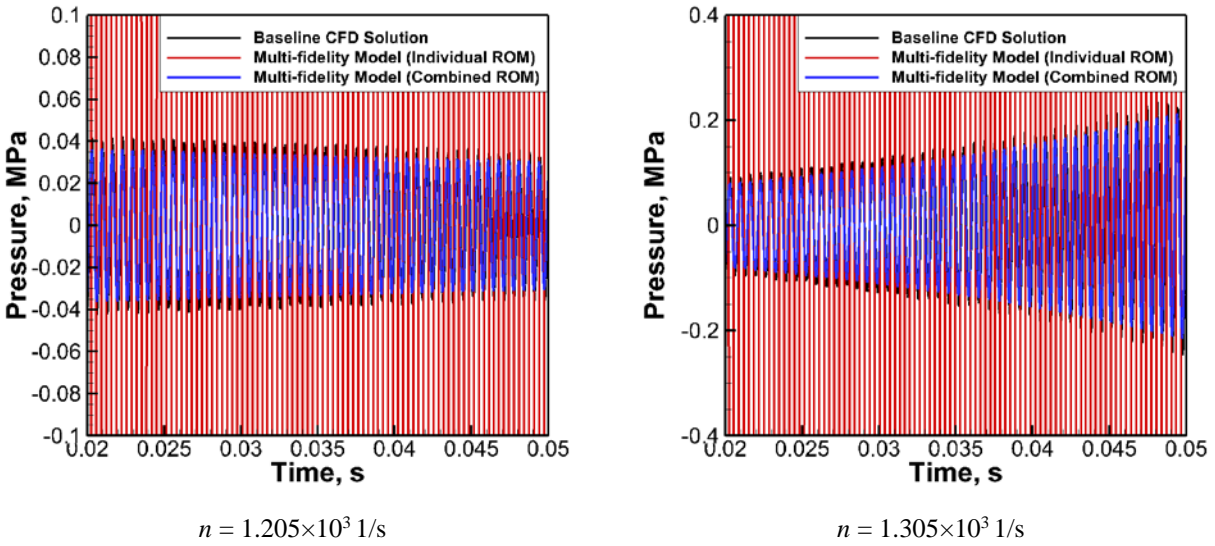


Figure 6. Comparisons of the predicted pressure fluctuations from baseline CFD and Multi-fidelity models using individual and combined ROMs corresponding to two different n values ($L_{ox} = 5.5''$ and $L_{chamber} = 15''$).

Two sets of ROM-based multi-fidelity solutions are also shown in Fig. 6. First, only the individual ROM trained by perturbing the inlet mass flow rate is integrated with the Euler solver following the framework procedures in Section III.C to predict the instability behaviors for a test problem (Fig. 1) However, the corresponding predicted solutions are highly unstable for both cases. Second, the complete set of ROMs (i.e., all three trained by perturbing different quantities at boundaries) are combined and integrated with the Euler solver for the model evaluations. It can be readily seen that the resulting predictions are able to match the baseline solution. We further note that ROMs trained by perturbing different boundary conditions either individually or in combinations of two (in other words, with an incomplete set of ROMs) does not yield the correct predictions. Good predictions are obtained only when the complete set of ROMs are used to represent the unsteady combustion response. The observation indicates the importance of developing comprehensive ROM combinations, which can provide the flame response for the corresponding input perturbation, so that the self-excited combustion instability can be captured correctly.

A. Reduced-domain ROM characteristics

The baseline test problems used for multi-fidelity framework evaluations are simulated to obtain distinguishable stability behaviors with the geometric and condition setup in Fig. 1 by varying the lengths of the post from 3.5'' to 11.5'' and applying different n values (from 0.605×10^3 to 1.405×10^3 1/s) in the n - τ model. The growth rates of the predicted pressure signals are computed for each case and the resulting baseline stability map is shown in Fig. 7 with positive growth rate representing unstable and negative representing stable combustion responses. A zero growth-rate solid black line is calculated to indicate the stability transition for the test problems. It can be seen that the cases

remain stable for all simulated n values at the two shortest post lengths (3.5'' and 4.5'') while the stability transition points shift toward lower n values as the post lengths increase.

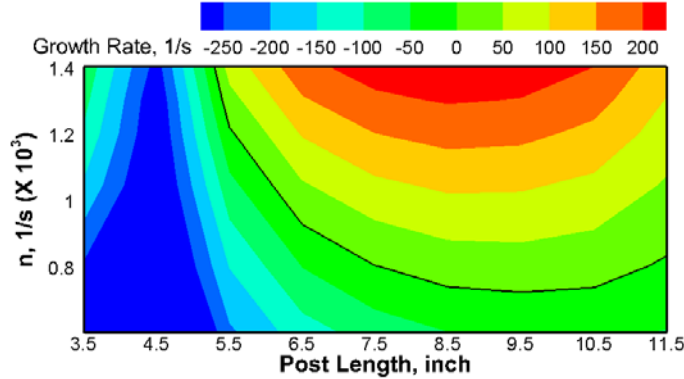
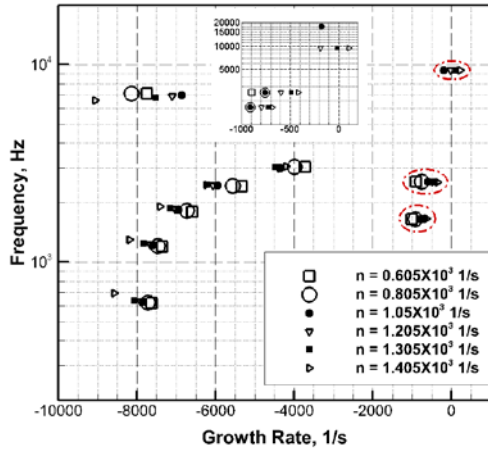


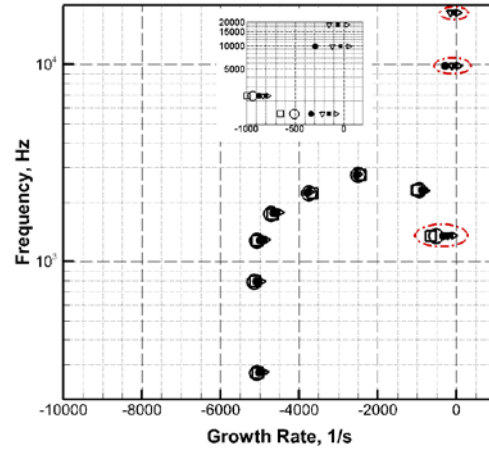
Figure 7. Stability map of baseline test problem simulations (positive growth rate (+): unstable and negative growth rate (-): stable).

Three reduced-domain geometries are simulated at consistent n values as the test problems (Fig. 7) to generate comprehensive sets of ROMs by perturbing either the upstream or downstream boundary conditions as concluded from Fig. 6. The geometries are setup as in Fig. 2 with $L_{ox} = 2.5''$ and different chamber lengths ($L_{chamber} = 5.5''$, $7.5''$ and $9.5''$).

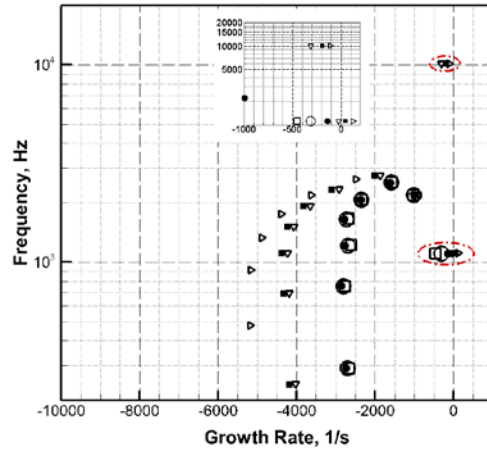
Before proceeding to evaluate the multi-fidelity model capabilities, it is necessary to investigate the characteristics of the resulting ROMs trained using different reduced-domain geometries. Therefore, the eigenvalue spectra of the ROMs trained by perturbing the inlet mass flow rate are computed for further studies and are shown in Fig. 8 with a zoomed-in view of selected modes for each training reduced-domain and n values that have been simulated. The generic system responses originated from the geometric effects of the reduced-domains are highlighted in dash-dotted red circle, the growth rates of which increase with the values of n as expected (i.e. the system becomes more unstable as n value get higher). The sympathetic responses here include the acoustic dynamics in the chopped chamber and oxidizer post in Fig. 2 (e.g. highlighted modes in between 1000 and 2000Hz represent chamber acoustics, the frequency of which decrease as the chamber lengths of reduced-domain get longer and the post acoustic modes can be seen in the spectrum of 5.5'' length chamber in between 2000 and 3000Hz) and injector responses driven by the post dynamics (e.g. high-frequency modes near 10kHz). More importantly, it should be noted that unstable modes (positive growth rate) can still be detected for high n values for each reduced-domain geometry even though an acoustically open boundary condition is applied (Fig. 2) to minimize the downstream wave reflections in the reduced chamber. These naturally unstable modes can be important in affecting the predictions from multi-fidelity model.



$L_{ox} = 2.5''$ and $L_{chamber} = 5.5''$



$L_{ox} = 2.5''$ and $L_{chamber} = 7.5''$



$L_{ox} = 2.5''$ and $L_{chamber} = 9.5''$

Figure 8. Eigen-value spectrum of ROM stiffness matrix at different n values using various reduced-domain geometries (ROMs trained by perturbing the inlet mass flow rate).

The predicted stability maps from the multi-fidelity framework approaches are shown in Fig. 9 with ROMs trained using different reduced-domain geometries. All three groups of ROMs are able to the overall trends of the stability transition with regards to different n values and post lengths. However, the multi-fidelity models with ROMs trained using reduced chamber of lengths 5.5'' and 9.5'' predict unstable behaviors at 4.5'' post length while it is supposed to be stable in terms of the baseline results (Fig. 7). This can be mainly attributed to the influences from the unstable modes with high growth-rate (>100 1/s) observed in the ROM spectra (Fig. 8). Although unstable modes can also be seen for the 7.5'' chamber reduced-domain ROM, the growth rates of the modes (~ 10 and 20 kHz) are lower (<100 1/s) than the other two cases so that the multi-fidelity modeling of the test problem is able to provide sufficient damping for these modes to overcome the growth. Moreover, it is noted that the existence of unstable modes seem to affect more on predicting the stable behaviors of the test problems than the unstable behaviors.

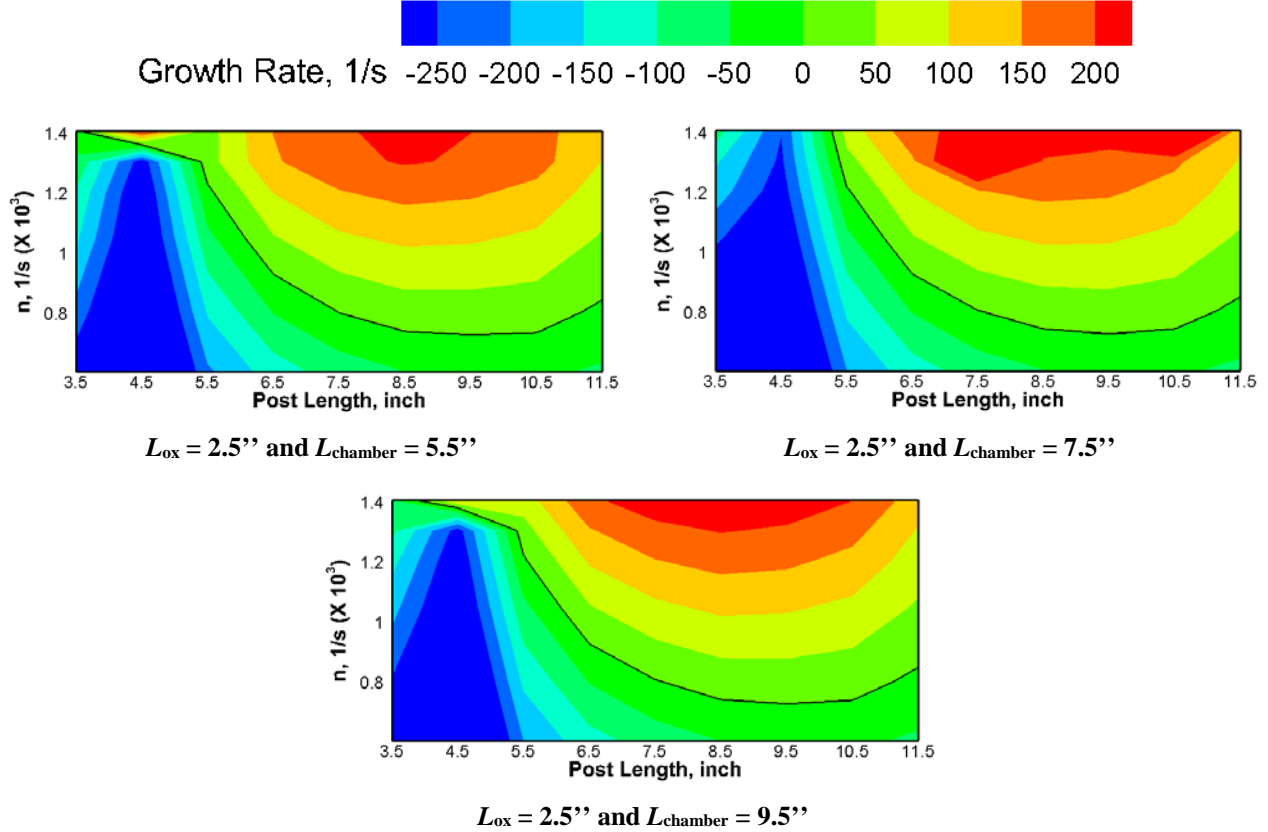


Figure 9. Stability maps of ROM-integrated multi-fidelity model simulations (positive growth rate (+): unstable and negative growth rate (-): stable, ROMs trained using different reduced-domain geometries).

Overall, the multi-fidelity framework approach proves to be capable of capturing the instability behaviors of the test problems though some discrepancies exist by using different reduced-domain geometries for the POD-based ROMs' training. A further issue that arises is the need to integrate multiple ROMs into the Euler solver, which involves a linear combination of the individual ROM results as described in Eq. (15). This creates some ambiguity in the formulation and, moreover, is likely to be valid only for linear problems. Therefore, to allow more flexibility and generality in the multi-fidelity framework, an alternative single-ROM approach based on utilizing the full injector configuration is considered next.

B. Full-injector-based ROM characteristics

In this section, we consider an alternate reduced-domain wherein the ROM is constructed for the entire injector post and only the length of the combustor is truncated. In this case, we note that a single-ROM can be constructed by perturbing only the downstream pressure boundary condition to represent the full injector response. The basic idea is as follows:

1. Instead of including a portion of the oxidizer post in the reduced-domain simulations for POD-based ROM training as in Fig. 2, the whole oxidizer post of the test problem is considered in the injector element for the reduced-domain simulations as shown in Fig. 10 with the same upstream boundary conditions as the test problem.

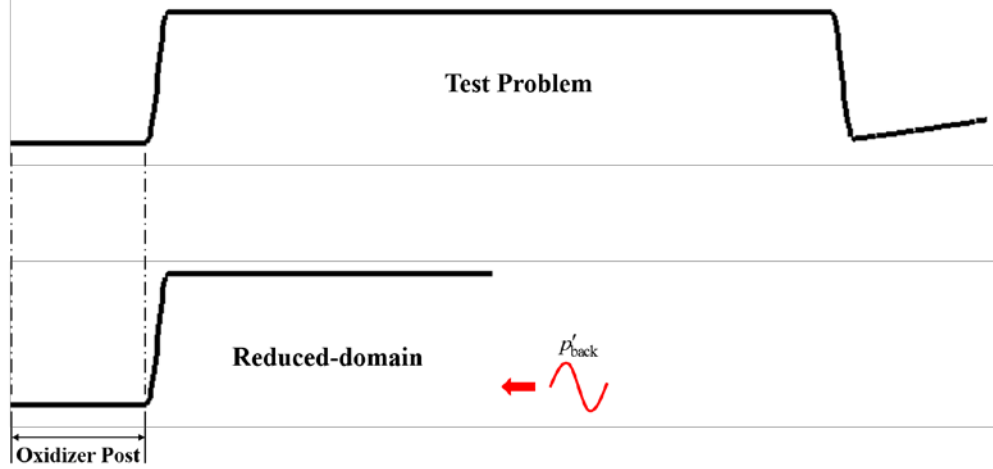


Figure 10. Descriptions of single-ROM approach proposed for the multi-fidelity framework.

2. Train the POD-based ROM by only perturbing the back pressure at downstream boundary and since the entire oxidizer post has been included in the reduced-domain simulations, the upstream dynamics in the oxidizer post is expected to respond correspondingly to the downstream perturbations, which enables the resulting ROM to provide the unsteady combustion responses coupling both upstream and downstream dynamics.

For the rest of the section, the proposed single-ROM approach is assessed by configuring the test problems with two fixed oxidizer post lengths ($L_{ox} = 5.5''$ and $3.5''$) and four varying chamber lengths ($L_{chamber} = 9''$, $11''$, $13''$ and $15''$) using different values of n . The same forcing function in Eq. (12) ($f_0 = 500\text{Hz}$, $= 250\text{Hz}$ and $N_f = 9$) as above is used to perturb the downstream back pressure for the ROM training.

The stability map comparisons between baseline and multi-fidelity models are shown in Fig. 11 for the test problem with fixed post length of $5.5''$. The growth rates of the predicted pressure signals are computed for each n value and chamber length with a zero growth-rate solid black line indicating the stability transition. It can be readily seen that the predictions of the stability behaviors from multi-fidelity model can reach good agreement with the baseline, which proves the validity of the proposed single-ROM approach.

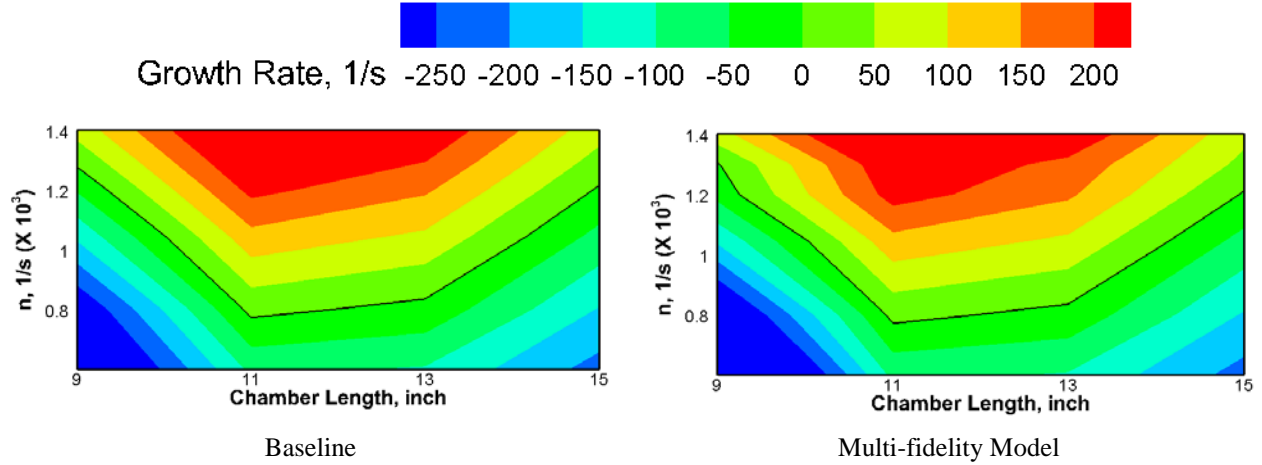


Figure 11. Stability maps comparisons between baseline and multi-fidelity simulations (fixed $L_{ox} = 5.5''$ and varying chamber lengths).

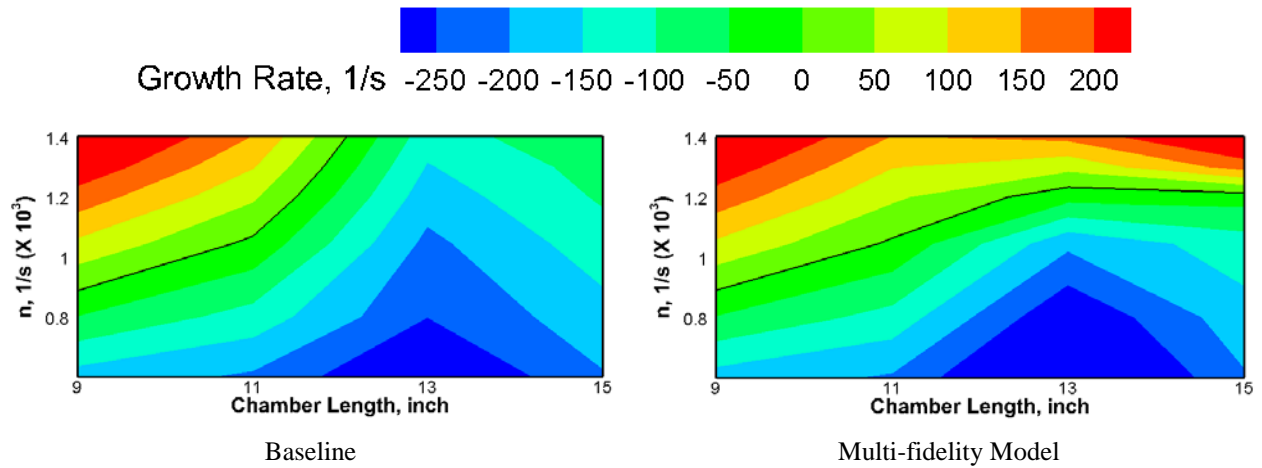


Figure 12. Stability maps comparisons between baseline and multi-fidelity simulations (fixed $L_{ox} = 3.5''$ and varying chamber lengths).

Similarly the stability map comparisons for test problem with the 3.5'' post length are shown in Fig. 12. In this case, the predictions from the multi-fidelity model are able to capture the instability behaviors for shorter chamber lengths (9'' and 11''); however, distinct discrepancies show up for longer chamber lengths (13'' and 15'') at higher n values (1.205×10^3 , 1.305×10^3 , and 1.405×10^3), which can be attributed to the existence of sympathetic unstable modes in the reduced-domain simulations for high n values. This observation is consistent with Section IV.A and the sympathetic unstable modes seem to impact the model predictions more for test problems with stable behaviors, which is the major reason why the multi-fidelity model provides better stability predictions for the 5.5'' post length than for the 3.5'' case.

V. Conclusions

A multi-fidelity framework for modeling combustion instability problems is established and assessed based on a linearized Euler solver. Simplified test problems for a model rocket combustor are simulated with the unsteady combustion response described by the n - τ model to provide benchmark solutions for evaluating the multi-fidelity framework's capabilities. The test problems are simulated by changing n values, that correspond to different levels of combustion response. Also various lengths of oxidizer post and combustion chamber are simulated so that different stable and unstable behavior can be obtained. The test problem is used as the basis for ROM model construction as well as for the validation of the resulting multi-fidelity model.

The overall procedure is as follows. A reduced-domain of the test problem involving only the main combustion region of the injector and combustor is utilized to train and construct suitable ROM's. Different reduced domains are formulated to determine the effects of the domain and the associated boundary conditions on the ROM. The final multi-fidelity framework that is used for the stability predictions is comprised of a linearized Euler solver with the combustion response obtained by the constructed ROM. In practical implementation, the reduced-domain calculations used to construct the ROM would be carried out using a high-fidelity LES or DES model, while the second set of predictive calculations would use the combined Euler-ROM framework to rapidly predict stability characteristics of the full injector-combustor configuration. In this paper, for demonstration purposes, both sets of calculations are carried out with the Euler equations.

Two types of reduced domains are considered in this paper. In both cases, the reduced domain contains the entire combustion region so that the ROM can adequately capture the combustion response of the injector. In the first scenario, the reduced domain contains only sections of the injector post and the combustor. This means that individual ROMs can be constructed by perturbing the different upstream and downstream boundary conditions. It is demonstrated that the multi-fidelity model is not able to reproduce the baseline stability behavior by using only one individual ROM (e.g., trained by perturbing upstream mass flow rate). Only when a complete set of ROMs is included in the framework, the model predictions are able to match the baseline stability characteristics. In addition, the effects of reduced-domain geometries on the predictive capabilities are investigated by varying the lengths of the reduced chamber ($L_{\text{chamber}} = 5.5'', 7.5''$ and $9.5''$). Overall, the predictions of the stability behaviors from the multi-fidelity model with all three ROMs show reasonable agreement with the baseline. However, some discrepancies are observed that can be attributed to unstable modes (growth rate > 0) originating from the generic system responses in the reduced-domain simulations.

In the second scenario, the entire oxidizer post is included in the reduced-domain simulations. A single-ROM is then trained by perturbing the downstream back pressure, while the upstream oscillations become naturally coupled with the downstream perturbations. This single-ROM approach allows more flexibility for implementing the multi-fidelity framework especially for nonlinear model problems. The single-ROM approach also shows that the multi-

fidelity model is generally successful in matching the baseline stability behavior. However, some discrepancies are again observed, which can be attributed to the unstable modes in the underlying ROM construction. Future work will consider ways to mitigate these effects. Further plans include the extensions of the multi-fidelity framework for non-linear problems as well as for multi-dimensional simulations.

References

1. Noiray, N., Durox, D., Schuller, T., and Candel, S. "A unified framework for nonlinear combustion instability analysis based on the flame describing function," *Journal of Fluid Mechanics* Vol. 615, 2008, p. 139.
2. Palies, P., Durox, D., Schuller, T., and Candel, S. "Nonlinear combustion instability analysis based on the flame describing function applied to turbulent premixed swirling flames," *Combustion and Flame* Vol. 158, No. 10, 2011, pp. 1980-1991.
3. Palies, P., Schuller, T., Durox, D., and Candel, S. "Modeling of premixed swirling flames transfer functions," *Proceedings of the Combustion Institute* Vol. 33, No. 2, 2011, pp. 2967-2974.
4. Schuller, T., Durox, D., and Candel, S. "A unified model for the prediction of laminar flame transfer functions," *Combustion and Flame* Vol. 134, No. 1-2, 2003, pp. 21-34.
5. Silva, C. F., Nicoud, F., Schuller, T., Durox, D., and Candel, S. "Combining a Helmholtz solver with the flame describing function to assess combustion instability in a premixed swirled combustor," *Combustion and Flame* Vol. 160, No. 9, 2013, pp. 1743-1754.
6. You, D., Huang, Y., and Yang, V. "A Generalized Model of Acoustic Response of Turbulent Premixed Flame and Its Application to Gas-Turbine Combustion Instability Analysis," *Combustion Science and Technology* Vol. 177, No. 5-6, 2005, pp. 1109-1150.
7. Popov, P. P., and Sirignano, W. A. "Transverse Combustion Instability in a Rectangular Rocket Motor," *Journal of Propulsion and Power*, 2016, pp. 1-8.
8. Morgan, C. J., Shipley, K. J., and Anderson, W. E. "Comparative Evaluation Between Experiment and Simulation for a Transverse Instability," *Journal of Propulsion and Power* Vol. 31, No. 6, 2015, pp. 1696-1706.
9. Harvazinski, M. E., Huang, C., Sankaran, V., Feldman, T. W., Anderson, W. E., Merkle, C. L., and Talley, D. G. "Coupling between hydrodynamics, acoustics, and heat release in a self-excited unstable combustor," *Physics of Fluids* Vol. 27, No. 4, 2015, p. 045102.
10. Lumley, J. L., and Poje, A. "Low-dimensional models for flows with density fluctuations," *Physics of Fluids* Vol. 9, No. 7, 1997, p. 2023.
11. Graham, W. R., Peraire, J., and Tang, K. Y. "Optimal Control of Vortex Shedding Using Low Order Models Part I: Open-Loop Model Development," *International Journal for Numerical Methods*, 1997.
12. Lucia, D. J., and Beran, P. S. "Projection methods for reduced order models of compressible flows," *Journal of Computational Physics* Vol. 188, No. 1, 2003, pp. 252-280.
13. Barbagallo, A., Dergham, G., Sipp, D., Schmid, P. J., and Robinet, J.-C. "Closed-loop control of unsteadiness over a rounded backward-facing step," *Journal of Fluid Mechanics* Vol. 703, 2012, pp. 326-362.
14. Barbagallo, A., Sipp, D., and Schmid, P. J. "Closed-loop control of an open cavity flow using reduced-order models," *Journal of Fluid Mechanics* Vol. 641, 2009, p. 1.
15. Barbagallo, A., Sipp, D., and Schmid, P. J. "Input-output measures for model reduction and closed-loop control: application to global modes," *Journal of Fluid Mechanics* Vol. 685, 2011, pp. 23-53.
16. Lieu, T., and Farhat, C. "Adaptation of Aeroelastic Reduced-Order Models and Application to an F-16 Configuration," *AIAA Journal* Vol. 45, No. 6, 2007, pp. 1244-1257.
17. Lucia, D. J., Beran, P. S., and Silva, W. A. "Reduced-order modeling: new approaches for computational physics," *Progress in Aerospace Sciences* Vol. 40, No. 1-2, 2004, pp. 51-117.
18. Munipalli, R., Zhu, X., Menon, S., and Hesthaven, J. "Model Reduction Opportunities in Detailed Simulations of Combustion Dynamics," *52nd Aerospace Sciences Meeting*. National Harbor, Maryland, 2014.

19. Huang, X., and Baumann, W. T. "Reduced-Order Modeling of Dynamic Heat Release for Thermoacoustic Instability Prediction," *Combustion Science and Technology* Vol. 179, No. 3, 2007, pp. 617-636.
20. Huang, C., Anderson, W. E., Merkle, C., and Sankaran, V. "Exploration of POD-Galerkin Method in Developing a Flame Model for Combustion Instability Problems," *7th AIAA Theoretical Fluid Mechanics Conference*. Atlanta, GA, 2014.
21. Huang, C., Anderson, W. E., Merkle, C., and Sankaran, V. "Exploration of POD-Galerkin Techniques for Developing Reduced Order Models of the Euler Equations," *51st AIAA/SAE/ASEE Joint Propulsion Conference*. Orlando, FL, 2015.
22. Huang, C., Anderson, W. E., Merkle, C., and Sankaran, V. "Investigation of the Stability of POD-Galerkin Techniques for Reduced Order Model Development," *54th AIAA Aerospace Sciences Meeting*. San Diego, 2016.
23. Crocco, L., Grey, J., and Harrjet, D. T. "On the Importance of Sensitivity Time Lag in Longitudinal High-frequency Rocket Combustion Instability," *Jet Propulsion* Vol. 28, No. 12, 1958, pp. 841-843.
24. Smith, R. J., Xia, G., Sankaran, V., Anderson, W. E., and Merkle, C. L. "Computational Investigation of Acoustics and Instabilities in a Longitudinal Mode Rocket Combustor," *AIAA Journal* Vol. 46, 2008.
25. Yu, Y. "Experimental and Analytical Investigations of Longitudinal Combustion Instability in a Continuously Variable Resonance Combustor (CVRC)," Doctor of Philosophy, Purdue University, 2009.
26. Yu, Y., Sisco, J. C., Rosen, S., Madhav, A., and Anderson, W. E. "Spontaneous Longitudinal Combustion Instability in a Continuously-Variable Resonance Combustor," *Journal of Propulsion and Power* Vol. 28, No. 5, 2012, pp. 876-887.